Research Article Vol. 7, No. 10 / October 2020 / Optica 1349

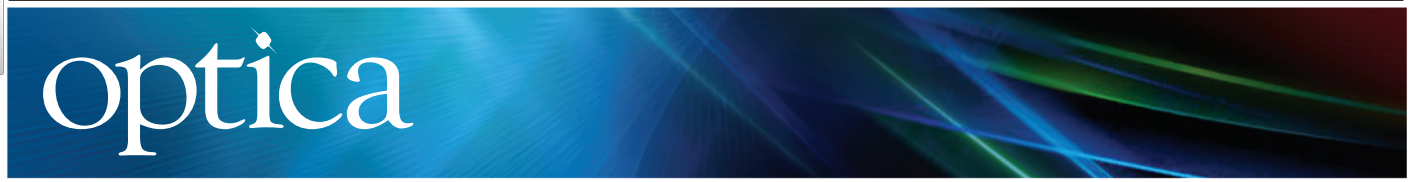

# Extreme Raman red shift: ultrafast multimode nonlinear space-time dynamics, pulse compression, and broadly tunable frequency conversion

P. A. Carpeggiani,[1,11,†] G. Coccia,[1] G. Fan,[1,2] E. Kaksis,[1] A. Pugžlys,[1,3] A. Baltuška,[1,3] R. Piccoli,[2,†] Y.-G. Jeong,[2] A. Rovere,[2] R. Morandotti,[2,4] L. Razzari,[2,9] B. E. Schmidt,[5] A. A. Voronin,[6,7] and A. M. Zheltikov[6,7,8,10]

[1]Institut für Photonik, Technische Universität Wien, Gußhausstrasse 27/387, 1040 Vienna, Austria
[2]Institut National de la Recherche Scientifique (INRS), Centre Énergie, Matériaux et Télécommunications (EMT), Varennes, Québec J3X 1S2, Canada
[3]Center for Physical Sciences and Technology, Savanoriu Ave. 231, LT-02300, Vilnius, Lithuania
[4]Institute of Fundamental and Frontier Sciences, University of Electronic Science and Technology of China, Chengdu 610054, Sichuan, China
[5]Few-Cycle Inc., 2890 Rue de Beaurivage, Montreal, Quebec H1L 5W5, Canada
[6]Physics Department, International Laser Center, M. V. Lomonosov Moscow State University, Moscow 119992, Russia
[7]Russian Quantum Center, Skolkovo, Moscow Region, 143025, Russia
[8]Department of Physics and Astronomy, Texas A&M University, College Station, Texas 77843, USA
[9]e-mail: razzari@emt.inrs.ca
[10]e-mail: zheltikov@physics.msu.ru
[11]e-mail:paolo.carpeggiani@tuwien.ac.at

Received 14 May 2020; revised 19 August 2020; accepted 23 August 2020 (Doc. ID 397685); published 8 October 2020

**Ultrashort high-energy pulses at wavelengths longer than 1 μm are now desirable for a vast variety of applications in ultrafast and strong-field physics. To date, the main answer to the wavelength tunability for energetic, broadband pulses still relies on optical parametric amplification (OPA), which often requires multiple and complex stages, may feature imperfect beam quality, and has limited conversion efficiency into one of the amplified waves. In this work, we present a completely different strategy to realize an energy-efficient and scalable laser frequency shifter. This relies on the continuous red shift provided by stimulated Raman scattering (SRS) over a long propagation distance in nitrogen-filled hollow-core fibers (HCF). We show a continuous tunability of the laser wavelength from 1030 nm up to 1730 nm with a conversion efficiency higher than 70% and high beam quality. The highly asymmetric spectral broadening, arising from the spatiotemporal nonlinear interplay between higher-order modes of the HCF, can be readily employed to generate pulses (∼20 fs) significantly shorter than the pump ones (∼200 fs) with high beam quality, and the pulse energy can further be scaled up to tens of millijoules. We envision that this technique, coupled with the emerging high-power Yb laser technology, has the potential to answer the increasing demand for energetic multi-TW few-cycle sources tunable in the near-IR.**



https://doi.org/10.1364/OPTICA.397685

## 1. INTRODUCTION

An increasing number of applications, such as attosecond pulse isolation via high-harmonic generation (HHG) [1], laser-induced field-driven electron emission [2], laser wakefield acceleration [3], laser-induced electron diffraction [4], optical coherence tomography [5], as well as ultra-broadband [6] and high-field [7] terahertz (THz) generation, have been shown to benefit from an increase in the driver pulse wavelength. For instance, the maximum photon energy generated via HHG [1] as well as the energy cutoff of field-driven, photo-emitted electrons [2] scale as $\lambda^2$, while the energy of ultrashort THz pulses generated via two-color plasma scales as $\lambda^{4.6}$ [6]. Regarding HHG, longer wavelengths extend the cutoff, but the overall efficiency drops with $\lambda^{-5}-\lambda^{-6}$, so each target spectral region has an optimal driver wavelength. For HHG in the water window (280–350 eV), the driver wavelength should be just above 1.2 μm [8]. Therefore, there is a growing interest in generating few-cycle, wavelength-tunable infrared fields, preferably with a stable carrier-envelope phase (CEP). Common laser media based on Ti, Yb, Nd, Cr, Er, and Tm ions, may generate ultrashort pulses, but at specific wavelengths: 800 nm, 1030 nm, 1064 nm, 1350 nm, 1500 nm, and 2000 nm, respectively. To date, the only viable solution that provides some degree of frequency tunability

relies on optical parametric amplification (OPA) in noncentrosymmetric materials (i.e., second-order nonlinear media featuring $\chi^{(2)}$) for frequency down-conversion [9,10]. Although in typical femtosecond OPA systems, the energy conversion efficiency from the pump to the frequency down-converted wave can reach up to 10% (signal or idler) [11,12], this approach presents several drawbacks. For instance, an OPA based on BBO or KTA nonlinear optical crystals and pumped by an Yb laser emitting at 1.03 μm can achieve continuous frequency tuning in the near-infrared region $>1.35-2.06$ μm for the signal (and $2.06-<4.5$ μm for the idler) with a "gap" in the spectrum between 1.03 μm and 1.35 μm that cannot be filled directly. This is because the transparency of the nonlinear crystal employed, the phase-matching condition, and the temporal matching required to efficiently transfer energy from the pump to the signal/idler set strict boundaries to the operation range. The spectral range between 1.03 μm and 1.35 μm via OPA can be attained either by doubling the pump frequency via second harmonic (SH) generation or by frequency doubling of the generated idler pulses; however, this happens at the expense of the overall efficiency. Typically, OPAs involve sequential cascaded frequency conversions and require multiple stages, impair beam quality, and deliver pulse durations comparable to the one of the pumping (or seeding) laser system. As an alternative, stimulated Raman scattering (SRS) [13] has firmly established itself as a versatile technique for pulse frequency conversion that enables, among other effects, a tunable soliton self-frequency shift in fibers [14], generation of optical attosecond pulses from a collection of Raman sidebands [15], and efficient Stokes-pulse generation in molecular gas cells pumped by narrowband pulses [16]. However, despite numerous attempts, in the case of broadband energetic pulses, the generation efficiency of SRS-converted ultrashort pulses does not exceed 15% [17]. A fundamental difficulty in increasing the energy and bandwidth of the pump pulses in the SRS scheme is that other nonlinear optical processes, such as self-phase modulation (SPM) and ionization, easily overtake the low-efficiency SRS interaction. Over the past two decades, hollow-core (capillary) fibers (HCF) have been extensively exploited for extreme pulse compression via nonlinear-induced spectral broadening, using both Raman-inactive noble gases [18–20] and molecular gases [21–24]. A gas-filled HCF is indeed an advantageous platform for extending the nonlinear optical interaction length to several meters with low/negligible dispersion. Moreover, because of the waveguiding geometry, the output beam profile has typically a very high quality. In this work we show that, by propagating ∼200 fs pulses delivered by Yb-based amplified laser systems (central wavelength of 1030 nm) in a $N_2$-filled HCF [Figs. 1(a) and 1(b)], an asymmetric spectral broadening toward longer wavelengths is observed [Figs. 1(c) and 1(d)]. Given the bandwidth of the laser systems employed in our investigation (∼3.8 THz at $1/e^2$ of the intensity), the interaction of the pulses with the $N_2$ gas is affected only by rotational modes (rotational constant $B = 0.06$ THz) and is not influenced by the vibrational ones ($\Delta\nu_{\mathrm{vib}} = 70$ THz) [25,26]. The red shift thus results from a cascaded Raman effect evolving during the long propagation (∼6 m) in the HCF. By simply adjusting the gas pressure, such a system grants the possibility of continuously red shifting the spectrum by as much as 300 nm [Fig. 1(c)] for our ∼10 mJ setup [Fig. 1(a)] and by 700 nm [Fig. 1(d)] for the ∼1 mJ setup [Fig. 1(b)]. We note that the commonly used one-dimensional (1D) pulse evolution model [27] cannot explain such impressive spectral asymmetry. Only a full

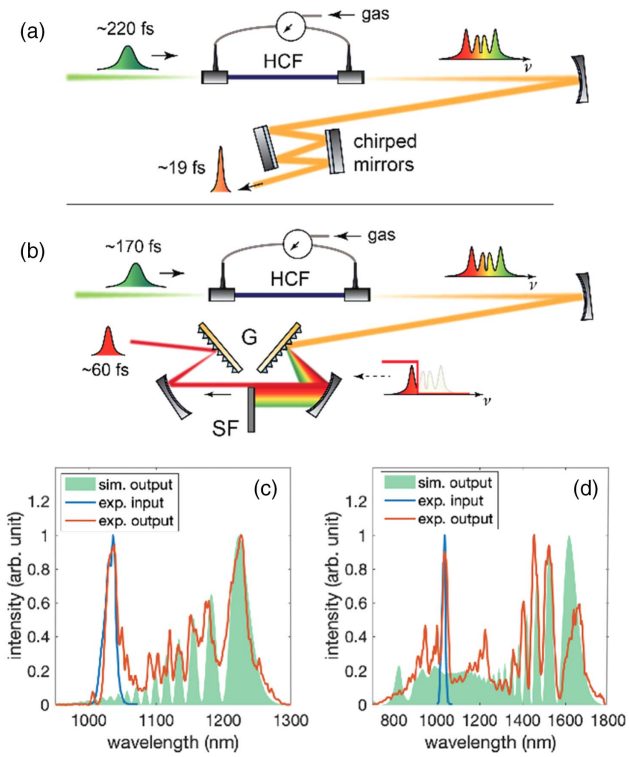


**Fig. 1.** Experimental setup and main results. (a) Experimental setup for ∼10 mJ pulses: the laser pulses propagate in a 5.5 m long, 1 mm inner diameter, stretched HCF and are subsequently compressed over the whole bandwidth with chirped mirrors. (b) Experimental setup for ∼1 mJ pulses: the laser pulses propagate in a 6 m long, 530 μm inner diameter, stretched HCF. The outer lobe on the red side of the spectrum is selected by spatial filtering in a 4 $f$-geometry monochromator. G, grating; SF, spatial filter. (c) Red shift for the setup in (a), obtained at 0.9 bar of $N_2$ pressure. (d) Red shift for the setup in (b), obtained at 4.0 bar of $N_2$ pressure. Experimental data, orange line. Simulations, green full curve. Input spectra, blue line. Intensities are normalized.

3D approach, including the spatiotemporal nonlinear dynamics between higher-order modes propagating in the HCF, can account for the spectral asymmetry observed in our experiments. In addition to frequency tuning, the obtained spectral broadening permits drastic pulse shortening via post-compression of the whole spectrum [Fig. 1(a)] or via spectral filtering [Fig. 1(b)]. This is especially important for Yb-based lasers. Indeed, the latter have been surpassing the well-established Ti:Sapphire systems in terms of overall efficiency and average output power (up to ∼10 kW), but are still limited to hundreds of femtosecond (at best) pulse durations [28]. Our strategy can straightforwardly deliver ultrashort pulses with high beam quality, wide frequency tunability, and scalable energy. This technique coupled with the emerging high-power femtosecond Yb laser technology, has the potential to satisfy the demand for multi-TW infrared few-cycle sources that are needed in many strong-field applications.

## 2. EXPERIMENTAL SETUPS

To provide a complete experimental investigation on the extreme Raman red shift observed in nitrogen-filled HCFs and explore an order of magnitude range of pulse energies and gas pressures, we employed different Yb laser systems available at the TUWien and at

the INRS-EMT. In particular, the two setups were used to demonstrate two different mechanisms to generate transform-limited sub-100 fs pulses: i) by compressing the whole output spectrum with chirped mirrors [Fig. 1(a)] and ii) by filtering an external lobe of the broadened spectrum to readily obtain continuously tunable pulses [Fig. 1(b)], respectively. In both cases, ∼200 fs pulses at 1.03 μm from the Yb-based amplified laser systems were coupled into upgraded, soft, stretched HCFs (few-cycle Inc., Montreal). Unlike conventional rigid HCFs, a soft HCF is stretched and kept straight by using specific holders. In this way, HCFs with lengths exceeding several meters can be used to enable high pulse compression ratios at significant (up to 80%) throughput levels. The focal spot size was adjusted to 64% of the fiber core diameter for optimum matching to the fundamental $EH_{11}$ mode [29], by properly tuning the distance between two mirrors in a telescope configuration. The focal spot was imaged on a CCD camera to measure the beam waist. The relative alignment of the laser beam and the HCF was achieved by maximizing the fundamental mode beam quality at the output as well as the overall power transmission of the fiber. At the TUWien [Fig. 1(a)], a home-built regenerative amplifier based on a cryogenically cooled Yb:$CaF_2$ delivering up to 14 mJ, 220 fs pulses at 2 kHz was used in combination with a 5.5 m long, 1 mm inner diameter HCF. A 50 Hz multipass Yb:$CaF_2$ laser amplifier was also used for testing input pulse energies up to 26 mJ. The output spectrum was recorded with an optical spectrum analyzer (AQ-6315A, Yokogawa Electric Corp., Tokyo) while the temporal characterization of the output pulses was performed via second harmonic generation, frequency-resolved optical gating (SHG-FROG) employing a 50 μm thick $\beta$-BBO crystal. The output pulses were recompressed with four bounces on broadband chirped mirrors featuring high reflectivity in the range 800–1200 nm (UltraFast Innovations GmbH, Munich) providing a group delay dispersion (GDD) of $-150$ $fs^2$ each. At the INRS-EMT [Fig. 1(b)] an Yb:KGW laser (PHAROS, Light Conversion, Vilnius, Lithuania) delivering up to 1 mJ, 170 fs pulses at 6 kHz was used in combination with a 6 m long, 530 μm inner diameter HCF. In this case, the output pulses were simply collimated by a concave mirror (focal length of 1 m) and filtered by means of a 4 $f$-geometry monochromator set at its zero-GDD point. The output spectra were measured combining two spectrometers covering the ranges 200–1000 nm and 1000–1800 nm (Avantes, Apeldoorn, The Netherlands). The recorded spectra were then corrected by considering the corresponding spectrometer sensitivities. The output pulses were temporally characterized via SHG-FROG (few-cycle Inc., Montreal) with a 50 μm thick $\beta$-BBO crystal.

## 3. THEORETICAL MODEL

The necessity to develop an adequate 3D propagation model becomes apparent from the shortcomings of the standard 1D model that fails to explain our experimental observations. (See Supplement 1 for detailed information on the theoretical model and physical scenario.) Because of the nearly instantaneous response, lowest-order Kerr nonlinearities cause a symmetric spectral broadening in the case of a symmetric pulse envelope. Correspondingly, the red and blue frequency components are generated at the leading and the trailing pulse edges, respectively. By contrast, the nonlinear phase induced by the Raman effect, due to the delayed response, is shifted toward the trailing edge of the pulse, thus enhancing the red shift. The standard 1D model [Fig. 4(c) in Supplement 1], even when it incorporates the Raman-related nonlinearity, predicts significantly more symmetrical broadening for our experimental parameters, thus contradicting our observations. This unusual and, in many ways, remarkable scenario of extreme spectral red shifting can be understood considering the complex sequence of strongly coupled ultrafast multimode spatiotemporal transformations of the ultrashort field waveforms in the gas-filled waveguide.

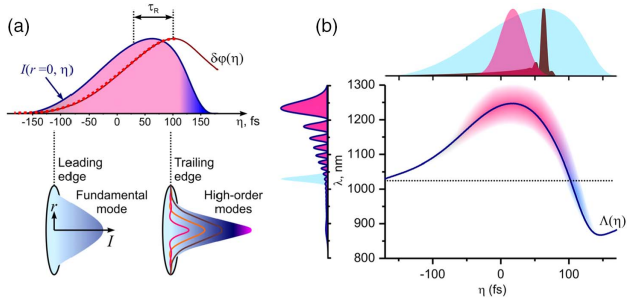


**Fig. 2.** Physics behind the extreme Raman red shift. (a) Field intensity envelope (blue solid line) with blue- and red-shifted sections shown by blue and red shading against the temporal phase (red solid line) with its growing part, corresponding to a red spectral shift and represented by red dots. The beam profiles in the leading (left) and trailing (right) edges of the pulse are also depicted. (b) Instantaneous wavelength Λ as a function of time $\eta$. The field intensity envelope of the fiber output (light blue), the compressed pulse (brown), and the fiber output transmitted through a 1450–1650 nm bandpass filter (red) are shown in the upper panel. The input spectrum (light blue) and the spectrum of the fiber output (red) are illustrated on the left panel.

Using a quasi-discrete Hankel transformation, the electric field is decomposed into the spatial modes supported by the waveguide [Eq. (1) in Supplement 1]. For the propagation, the delayed Raman response and the instantaneous response due to the Kerr nonlinearity (up to $n_4$) are taken into account [Eq. (2) in Supplement 1], together with the dispersion operator, propagation constant, and leakage loss of each individual mode. We verified numerically that the ionization term contributes less than 0.1% to the cumulative nonlinear phase shift, dominated by the SPM and the SRS terms; therefore, it can be considered as insignificant. Following the treatment of nonlinear propagation in discrete spatial modes, the total electric field is then reassembled by means of Hankel transformations.

Solving Eq. (2) of Supplement 1, it is shown that the total nonlinear phase is not uniform both in time (within the pulse envelope) and space (across the beam profile), thus giving rise to a time-dependent nonlinear lens. This lens is responsible for the excitation of higher-order waveguide modes, especially in the trailing edge of the pulse under the combined effect of the delayed Raman response and self-steepening. The walk-off of the modes due to their group velocity mismatch adds to the drastic drop of the field intensity on the trailing edge and increases its lag with respect to the nonlinear phase shift. As a result, the generation of the blue spectral wing is further inhibited [Fig. 2(a)]. New red spectral components generated at different times result in a characteristic interference pattern in the spectrum [Fig. 2(b)], visible both in the experiments and in the theory.

The validity of the model is confirmed by the agreement between simulations and experimental results, for both the spectral and temporal properties of the red-shifted pulses.

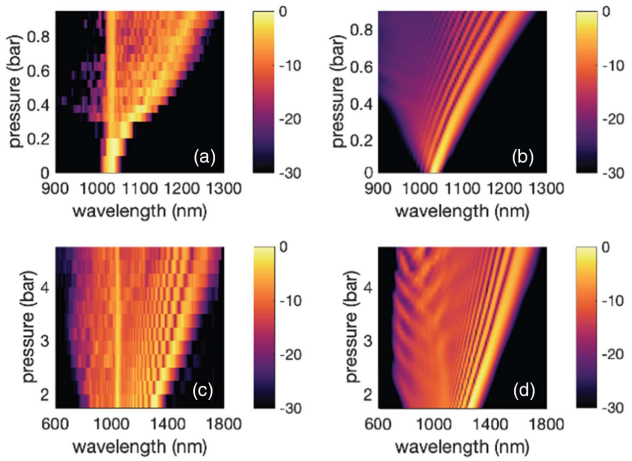


**Fig. 3.** Spectral broadenings. Spectra of the fiber output: (a) and (b) measured and (c) and (d) calculated as a function of the $N_2$ pressure inside the fiber for (a) and (c) $W = 10$ mJ, $\tau = 220$ fs, $d = 1.0$ mm and $L = 5.5$ m, and for (b) and (d) $W = 1$ mJ, $\tau = 170$ fs, $d = 0.53$ mm and $L = 6.0$ m.

## 4. EXPERIMENTAL RESULTS

### A. Spectral Characterization

For ∼10 mJ input pulses in combination with the 1 mm inner diameter fiber, a spectral red shift (defined at the $1/e^2$ level of the peak of the last lobe) up to 1.28 μm was observed, while a shift up to 1.73 μm for ∼1 mJ pulses coupled to the 530 μm fiber was measured, as shown in Figs. 1(c) and 1(d). Up to 82% and 72% of the energy is transferred from the fundamental to longer wavelengths in the first and in the second case, respectively (as calculated by considering the output energy located beyond 1050 nm with respect to the total energy coupled into the waveguide). A broad and continuous tunability of the laser spectral content can be obtained by simply varying the gas pressure, as shown in Fig. 3. Figures 3(a) and 3(b) illustrate the measured spectral broadenings as a function of the gas pressure. As can be seen, the laser spectrum asymmetrically evolves toward longer wavelengths and well-defined spectral lobes, similar to the ones observed in the SPM process, are clearly visible. Figures 3(c) and 3(d) show the corresponding numerical simulations, which are found to be in good agreement with the experimental results. The different spectral broadenings observed in the two experiments are well understood considering the scaling law introduced in [30], where it was demonstrated that the broadening induced by SPM scales as $\Delta\omega \propto L/A \cdot P \cdot k_2 p/\lambda_0^2$. Here, $L$ is the length of the fiber, $A$ the section area, $P$ is the pulse peak power, $\lambda_0$ is the central wavelength, and $k_2$ is the ratio between the nonlinear index coefficient and the gas pressure $p$. Even though in our case SRS is the dominant process, we can assume—in a first approximation—the same dependence. The results of the two experimental setups, are obtained with:

(i) 10 mJ, 220 fs, 0.9 bar, 1 mm inner diameter, and 5.5 m HCF length and
(ii) 1 mJ, 170 fs, 4.0 bar, 530 μm inner diameter, 6 m HCF length,

and can be compared to this scaling law to obtain a ratio of 1:2, which well corresponds to the experimentally measured 57 THz and 115 THz red shifts, respectively. Similar to the case for SPM, the maximum broadening for SRS is limited by the ionization of the gas and by the critical power for self-focusing $P_{cr} = \lambda_0^2/(2k_2 p)$.

The pulse energy $W$ scaling requires larger $A \propto W$ to keep the laser intensity below the limit of ionization of the gas. Because of the critical power limit, the product $P \cdot p$ must be kept constant; thus $L$ should scale as $L \propto A \propto W$ to achieve the same $\Delta\omega$.

Given the limits of a setup in terms of length, these conditions imply that for (SPM) SRS there is a trade-off between the maximum (broadening) shift and the pulse energy.

When comparing the experimental spectra and the simulations, the only noticeable difference is the persistence of the fundamental wavelength in the data from both setups. This might be due to its propagation in higher-order modes that are above the simulation limit, thus resulting in different output spatial distributions. Nevertheless, it will be shown in the next section and in Supplement 1 that the fundamental wavelength does not affect nonlinear applications such as SHG-FROG.

### B. Temporal Characterization

Two possible techniques were considered for the production of pulses significantly shorter than those of the respective input lasers:

(i) compressing the whole spectrum with broadband chirped mirrors [Fig. 1(a)] and
(ii) spectrally selecting the external lobe of the red shifted spectrum by spatially filtering it with a $4f$-geometry monochromator set at the zero-GDD point [Fig. 1(b)].

The first approach, explored at the TUWien, is suitable for strong-field experiments and HHG. Indeed, the center of mass of the output spectrum shifts toward longer wavelengths with respect to the input, while the total output energy is mostly retained, thus potentially delivering multi-mJ, TW-level peak power pulses. To demonstrate the compressibility of the Raman-chirped pulse, we first measured the uncompressed output via SHG-FROG [Fig. 4(a)] and simulated the corresponding SHG-FROG trace [Fig. 4(b)]. As shown, the experimental results and simulations are in very good agreement. They illustrate highly asymmetric (along the wavelength axis) SHG-FROG traces, further validating the negligible generation of light at wavelengths shorter than that of the input laser. Besides the asymmetry, the pattern closely resembles that of an ideal SPM process, supporting the possibility of compressing the output pulse by simply applying negative GDD. The retrieved output uncompressed pulse is shown in Fig. 4(c) (green) together with the input laser pulse (blue). By exploiting the partial spectral overlap (from 1030 to 1170 nm) between the output uncompressed pulse and the broadband chirped mirrors, we generated 19 fs, 6.5 mJ pulses centered at 1120 nm. By finely tuning through the laser compressor the second- and third-order spectral phase of the input pulse while monitoring the output SHG-FROG signal, it is possible to concentrate most of the energy in the main peak [Fig. 4(c), red]. Figure 4(d) illustrates the corresponding pulse obtained from numerical simulations (see Supplement 1 for detailed information). Analogously to the experimental results, the input (blue) and output uncompressed (green) pulses show similar durations. When introducing the GDD of the chirped mirrors in the simulation, as shown by the short-dashed black line in Fig. 4(e), the output pulse can be compressed down to approximately 18 fs [red and dashed black lines in Fig. 4(d)], which is in good agreement with the experimental results. When approximated with a Lorentzian profile, as shown by the light blue shading in Figs. 4(c) and 4(d), the pulse carries 80% of the total energy. The uncompressed and compressed simulated pulses

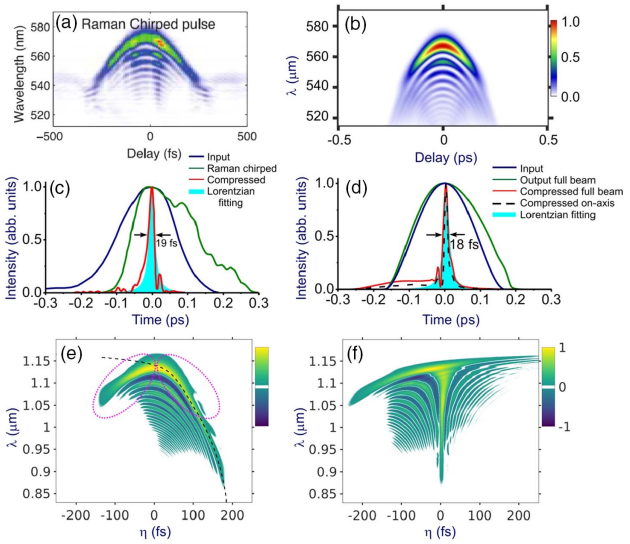


**Fig. 4.** Compression of the pulses after the HCF with an inner diameter $d = 1$ mm and length $L = 5.5$ m, filled with $N_2$ at a pressure $p = 0.6$ bar, for an output pulse with an energy $W = 6.5$ mJ and a width $\tau = 220$ fs. (a) Experimental and (b) simulated SHG-FROG traces of the pulse at the output of the fiber, (c) temporal envelopes of the input (blue), output (green), and compressed (red) pulses retrieved from the experimental SHG-FROG traces. (d) Simulated temporal envelopes of the pulse at the fiber output integrated over the beam (green) and compressed pulse on the beam axis (dashed black line) and integrated over the beam profile (red) against the input pulse envelope used in the model (blue). (e) and (f) Simulated Wigner maps for (e) the pulse at the fiber output and (f) the compressed pulse. Interfering field components are contoured by fuchsia dotted lines. The simulated dispersion of the chirped mirrors is also shown (short dashed black line).

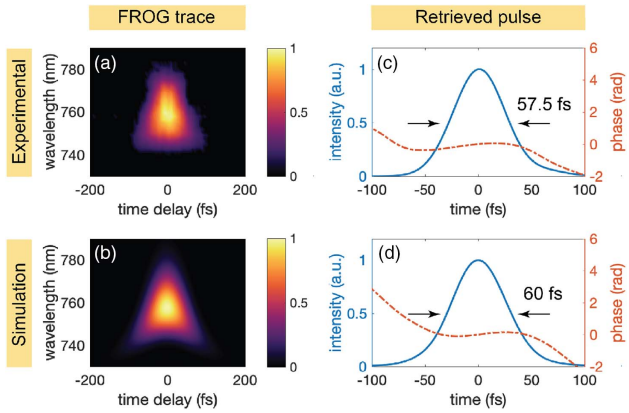


**Fig. 5.** Temporal characterization of the filtered external lobe of the spectrum. (a) Experimental and (b) simulated SHG-FROG traces of the fiber output transmitted through a 1450–1650-nm-bandpass filter. Input pulses with energy $W = 0.9$ mJ and pulse-width $\tau = 170$ fs are transmitted through an HCF with an inner diameter $d = 0.53$ mm and length $L = 6.0$ m, filled with $N_2$ at a pressure $p = 3.4$ bar. (c) and (d) Temporal envelopes (solid blue lines) and temporal phases (dotted orange lines) retrieved from the (a) experimental and (b) simulated SHG-FROG traces, respectively.

are also displayed in the Wigner representation in Figs. 4(e) and 4(f), respectively, which provides a convenient way to visualize the spectral components of the pulse in time. The two dotted fuchsia contour lines in Fig. 4(e) identify the pulse components that share the same wavelength, but are generated at different times. Since the relative phase of these components varies with the wavelength, their interference gives rise to well-resolved fringes that result in the typical pattern clearly visible in the spectra of Figs. 1(c), 1(d), 2(b), and 3. After compression [Fig. 4(f)], the spectral components of the pulse are located at the same time, thus forming the intense 18 fs pulse [Fig. 4(d)]. Further tests at higher energy (26 mJ), with a lower repetition rate, allowed us to get an output of 20 mJ (76%) from the fiber, of which we estimated that 14 mJ (70%) were compressed below 20 fs (see Supplement 1 and Fig. S6) corresponding to a 0.7 TW peak power. It is worth emphasizing that the use of chirped mirrors covering the whole available bandwidth of the red-shifted spectrum would further improve the pulse compression quality.

With the second approach, explored at the INRS-EMT, quasi-Fourier-limited pulses can be directly generated (Fig. 5) by simply filtering the most red-shifted lobe of the output spectrum. Although this method does not retain the full output energy, it represents a simple and convenient way to deliver widely tunable sub-100 fs pulses in the near-IR with energy conversion efficiencies (input–output) comparable to those of commercially available OPA systems. This is possible since, analogously to the case of pure SPM [27], the spectral phase over the individual lobes assumes a quasi-linear dependence over the frequency, which in turn results in a simple temporal shift of the corresponding pulse. As a proof of principle, we selected the external lobe of the output spectrum reached at 3.4 bar $N_2$ pressure and 0.9 mJ pulse energy, with a full width at half maximum of 73 nm centered at 1510 nm (see Supplement 1 and Fig. S7). This was achieved in the experiments by spatially filtering the beam in a 4f-geometry monochromator [see Fig. 1(b)] and in the simulation by applying an equivalent 1450–1650-nm bandpass filter. Figures 5(a) and 5(b) show the SHG-FROG traces of the filtered external lobe in the experiment and simulation, respectively. Figures 5(c) and 5(d) illustrate the corresponding retrieved pulses, highlighting a very good agreement between the experimental result and the simulation. As shown, the well-behaved spectral modulation that can be achieved with $N_2$ allows us to straightforwardly obtain well-shaped ~57 fs pulses (a time-bandwidth product of 0.55) with conversion efficiency (input–output) of about ~8%. With the same approach, it was possible to isolate pulses with similar temporal features, but centered at 1200 nm, 1300 nm, 1400 nm, and 1600 nm. Indeed, this approach guarantees continuous tunability by simply varying the gas pressure in the HCF [as shown in Fig. 3(b)]. Furthermore, the same strategy can also be used to access the mid-IR domain with stable CEP, by selecting two lobes of the red-shifted spectrum and performing difference-frequency generation (DFG) in a nonlinear crystal. DFG tuning could be achieved by adjusting the phase matching and the time delay between the corresponding pulses.

## 5. CONCLUSIONS

In conclusion, we have demonstrated what we believe is a highly attractive energy-scalable approach to develop wavelength-tunable drivers for strong-field applications. More than 70% of the energy of 200 fs, 1030 nm pulses can be transferred into the near-IR spectral domain extending up to 1.73 μm. This breakthrough is enabled by the use of large core diameter, multimeter HCFs that, in combination with relatively long input laser pulses and Raman-active gases, provide conditions to promote a distinctive cascaded SRS process over other nonlinear interactions such as SPM. We

have shown that the Raman-shifted output spectrum can be compressed with broadband chirped mirrors to obtain few-cycle pulses in the near-IR, or simply filtered to obtain wavelength-tunable ~60 fs long pulses. We believe that this technique offers a convenient alternative to the more demanding OPA systems to achieve gap-free tuning in the near-IR, while it may also grant access to the visible domain by SHG, as well as to the mid-IR by performing DFG between different lobes of the output spectrum. Moreover, such an approach can be upscaled into the TW regime with the current setup, and an even shorter pulse duration is expected with chirped mirrors covering the entire available spectrum. We envision that the proposed method, coupled with the emerging high-power Yb laser technology, has the potential to answer the increasing demand for long-wavelength, multi-TW few-cycle sources needed in many strong-field applications.

**Funding.** Natural Sciences and Engineering Research Council of Canada; PROMPT Quebec; Austrian Science Fund (P27491); Russian Foundation for Basic Research (18-02-40034, 18-29-20031, 18-32-20196, 19-02-00473); Welch Foundation (A-1801-20180324); Russian Science Foundation (20-12-00088—multioctave nonlinear optics).

**Acknowledgment.** The authors thank Prof. Marco Marangoni from Politecnico di Milano for the useful discussion. R. Morandotti is affiliated with the University of Electronic Science and Technology of China as an adjoint faculty.

**Disclosures.** The authors declare no conflicts of interest.

See Supplement 1 for supporting content.

[†]These authors contributed equally to this work.

## REFERENCES

1. P. B. Corkum and F. Krausz, "Attosecond science," Nat. Phys. **3**, 381 (2007).
2. G. Herinck, D. R. Solli, M. Gulde, and C. Ropers, "Field-driven photoemission from nanostructures quenches the quiver motion," Nature **483**, 190 (2012).
3. C. W. Siders, T. Galvin, A. C. Erlandson, and A. Bayramian, "Wavelength scaling of laser wakefield acceleration for the EuPRAXIA design point," Instruments **3**, 44 (2019).
4. M. G. Pullen, B. Wolter, A.-T. Le, M. Baudisch, M. Hemmer, A. Senftleben, C. D. Schröter, J. Ullrich, R. Moshammer, C. D. Lin, and J. Biegert, "Imaging an aligned polyatomic molecule with laser-induced electron diffraction," Nat. Commun. **6**, 7262 (2015).
5. N. M. Israelsen, C. R. Petersen, A. Barh, D. Jain, M. Jensen, G. Hannesschläger, P. Tidemand-Lichtenberg, C. Pedersen, A. Podoleanu, and O. Bang, "Real-time high-resolution mid-infrared optical coherence tomography," Light Sci. Appl. **8**, 11 (2019).
6. M. Clerici, M. Peccianti, B. E. Schmidt, and L. Caspani, "Wavelength scaling of terahertz generation by gas ionization," Phys. Rev. Lett. **110**, 253901 (2013).
7. C. Vicario, B. Monoszlai, M. Jazbinsek, S.-H. Lee, O.-P. Kwon, and C. P. Hauri, "Intense, carrier frequency and bandwidth tunable quasi single-cycle pulses from an organic emitter covering the terahertz frequency gap," Sci. Rep. **5**, 14394 (2015).
8. Y. Pertot, C. Schmidt, M. Matthews, and A. Chauvet, "Time-resolved x-ray absorption spectroscopy with a water window high-harmonic source," Science **355**, 264–267 (2017).
9. C. Manzoni and G. Cerullo, "Design criteria for ultrafast optical parametric amplifiers," J. Opt. **18**, 103501 (2016).
10. A. Ciriolo, M. Negro, M. Devetta, and E. Cinquanta, "Optical parametric amplification techniques for the generation of high-energy few-optical-cycles IR pulses for strong field applications," Appl. Sci. **7**, 265 (2017).
11. Light Conversion, Vilnius, Lithuania, http://lightcon.com/.
12. Coherent, Inc., Santa Clara, CA, USA, https://www.coherent.com/.
13. C. V. Raman and K. S. Krishnan, "A new type of secondary radiation," Nature **121**, 501 (1928).
14. Q. Lin and G. P. Agrawal, "Raman response function for silica fibers," Opt. Lett. **31**, 3086–3088 (2006).
15. A. Sokolov and S. Harris, "Subfemtosecond pulse generation by molecular modulation," Phys. Rev. Lett. **81**, 2894 (1998).
16. G. B. Jarvis, S. Mathew, and J. E. Kenny, "Evaluation of Nd:YAG-pumped Raman shifter as a broad-spectrum light source," Appl. Opt. **33**, 4938–4946 (1994).
17. C. Vicario, M. Shalaby, A. Konyashchenko, L. Losev, and C. P. Hauri, "High-power femtosecond Raman frequency shifter," Opt. Lett. **41**, 4719–4722 (2016).
18. M. Nisoli, S. De Silvestri, and O. Svelto, "Generation of high energy 10 fs pulses by a new pulse compression technique," Appl. Phys. Lett. **68**, 2793 (1996).
19. Y.-G. Jeong, R. Piccoli, D. Ferachou, V. Cardin, M. Chini, S. Hädrich, J. Limpert, R. Morandotti, F. Légaré, B. E. Schmidt, and L. Razzari, "Direct compression of 170-fs 50-cycle pulses down to 1.5 cycles with 70% transmission," Sci. Rep. **8**, 11794 (2018).
20. G. Fan, T. Balčiūnas, T. Kanai, T. Flöry, G. Andriukaitis, B. E. Schmidt, F. Légaré, and A. Baltuška, "Hollow-core-waveguide compression of multi-millijoule CEP-stable 3.2 um pulses," Optica **3**, 1308–1311 (2016).
21. N. Zhavoronkov, "Efficient spectral conversion and temporal compression of femtosecond pulses in $SF_6$," Opt. Lett. **36**, 529–531 (2011).
22. E. Haddad, R. Safaei, A. Leblanc, R. Piccoli, Y.-G. Jeong, H. Ibrahim, B. E. Schmidt, R. Morandotti, L. Razzari, F. Légaré, and P. Lassonde, "Molecular gases for pulse compression in hollow core fibers," Opt. Express **26**, 25426–25436 (2018).
23. C. Li, K. P. M. Rishad, P. Horak, Y. Matsuura, and D. Faccio, "Spectral broadening and temporal compression of ~100 fs pulses in air-filled hollow core capillary fibers," Opt. Express **22**, 1143–1151 (2014).
24. J. E. Beetar, M. Nrisimhamurty, T.-C. Truong, G. C. Nagar, J. Nesper, O. Suarez, Y. Wu, B. Shim, and M. Chini, "Multioctave supercontinuum generation and frequency conversion based on rotational nonlinearity," Sci. Adv. **6**, eabb5375 (2020).
25. A. M. Zheltikov, "An analytical model of the rotational Raman response function of molecular gases," J. Raman Spectrosc. **39**, 756 (2008).
26. https://hitran.org/.
27. G. Agrawal, "Nonlinear fiber optics," in *Optics and Photonics*, 5th ed. (Academic, 2013).
28. C. J. Saraceno, "Mode-locked thin-disk lasers and their potential application for high-power terahertz generation," J. Opt. **20**, 044010 (2018).
29. E. A. J. Marcatili and R. A. Schmeltzer, "Hollow metallic and dielectric wave-guides for long distance optical transmission and lasers," Bell Syst. Tech. J. **43**, 1783 (1964).
30. C. Vozzi, M. Nisoli, G. Sansone, S. Stagiram, and S. De Silvestri, "Optimal spectral broadening in hollow-fiber compressor system," Appl. Phys. B **80**, 285 (2005).